

Enhanced Photoluminescence from Very Thin Double-Wall Carbon Nanotubes Synthesized by the Zeolite-CCVD Method

Naoki Kishi,[†] Satoshi Kikuchi,[†] Palanisamy Ramesh,[‡] Toshiki Sugai,^{†,‡}
Yasuyuki Watanabe,[§] and Hisanori Shinohara^{*,†,‡}

Department of Chemistry and Institute for Advanced Research, Nagoya University, Nagoya 464-8602, Japan,
CREST, Japan Science and Technology Agency, c/o Department of Chemistry, Nagoya University,
Nagoya 464-8602, Japan, and Analytical & Measuring Instruments Division, Shimadzu Corporation,
Kyoto 604-8511, Japan

Received: May 3, 2006; In Final Form: July 31, 2006

Photoluminescence (PL) from purified (>90%) double-wall carbon nanotubes (DWNTs), which have been synthesized by zeolite catalyst-supported chemical vapor deposition (zeolite-CCVD), of very small diameters (0.8-nm average inner tube) is reported. The PL contour mappings for various ratios (1–90%) of double- versus single-wall carbon nanotubes by thermal oxidation have enabled us to unambiguously identify the chirality of inner tubes for the DWNTs synthesized. After the extensive high-temperature oxidation at 700 °C, high-purity (>90%) DWNTs of ~0.8 nm inner diameter are obtained, and most of these correspond to the DWNTs having inner tubes with chiralities of (7,5), (7,6), and (9,4).

Introduction

Double-wall carbon nanotubes (DWNTs) have attracted much attention during the past several years as a special class of carbon nanotube materials.^{1–13} DWNTs are the thinnest member of multiwall carbon nanotubes (MWNTs), which have a preferred structure for investigating interlayer interaction. For example, field emission studies have revealed that DWNTs are able to deliver stable emission current under low turn-on voltages with long lifetimes comparable to those of multiwall carbon nanotubes (MWNTs).⁹ DWNTs have exhibited an excellent sub-threshold swing (*S*) factor as compared with those of single-wall carbon nanotubes (SWNTs) when they are used for field effect transistor (FET) channels.¹⁰ These promising applications of DWNTs have accelerated the research activities on selective syntheses of DWNTs during the past several years.

Photoluminescence (PL) from SWNTs has attracted attention in recent years as a new way to investigate their fundamental optical and electronic properties.^{14–21} Excitation and emission energies of a PL peak correspond to E_{22}^s (the second van Hove singularity gap of semiconductor) and E_{11}^s (the first van Hove singularity of semiconductor) of an individual SWNT, respectively. Recent experimental studies have demonstrated that these optical transitions are dominated by excitonic recombination.²¹ PL mapping, which is a two-dimensional map of PL intensity as a function of emission and excitation wavelength, can provide important information on the chirality distribution of a carbon nanotube (CNT) sample.^{15,16} Hertel et al. reported PL from inner tubes of DWNTs synthesized by catalyst-supported chemical vapor deposition (CCVD) on MgO based materials.¹¹ Obtaining PL from pure DWNTs has not been, however, realized because of the difficulty to separate PL peaks of SWNTs from those of

DWNTs, because diameter distributions of inner tubes of DWNTs and SWNTs are normally overlapped.

Here, we report the photoluminescence from inner tubes of pure (>90%) DWNTs grown by the zeolite-CCVD method. To confirm that the observed PL is exclusively from DWNTs, we have investigated PL contour mappings at various relative ratios of DWNT versus SWNT and are able to identify the PL signals from purified DWNTs. This leads to an unambiguous chirality assignment for the inner tubes of DWNTs investigated.

Experimental Section

CCVD^{2–8,22–27} is one of the promising ways to selectively synthesize DWNTs.^{2–8} We have already reported the selective synthesis of DWNTs on zeolite and mesoporous silica^{6,8} supports by using CCVD. In the present study, DWNTs together with SWNTs were synthesized by CCVD with zeolite as support materials. Fe/Co (2.5/2.5 wt %) catalyst particles supported on a Y-type zeolite (HSZ390-HUA, Tosoh) were used as catalyst metal. DWNTs/SWNTs mixed samples were synthesized by using ethanol vapor²⁷ at 900 °C. The alcohol CCVD provides the SWNT rich sample. Commercially available HiPco-SWNT (CNI, purified) was also used for comparison.

Thermal oxidation is a convenient and important way to separate/purify DWNTs against SWNTs because of their much higher chemical resistance toward oxidation.^{1,5} It is also known that SWNTs with smaller diameters are more reactive toward oxidation than thicker tubes^{28,29}

By using this thermal method, we were able to obtain mixture samples of DWNT and SWNT at various ratios (1–90%) together with pure (ca. 90%) DWNTs by varying oxidation temperature. As-grown samples were oxidized in air at 520–720 °C for 30 min at a heating rate of 10 °C/min using a high-temperature oven.

DWNTs/SWNTs micelled solutions were prepared by a procedure similar to that of O'Connell et al.¹⁴ The mixed samples were dispersed in D₂O with 100 mM sodium cholate^{11,17,20} by using a 30 W ultrasonicator (Branson, Sonifier

* Author to whom correspondence should be addressed. Phone: +81-52-789-2482; fax: +81-52-789-1169; e-mail: noris@cc.nagoya-u.ac.jp.

[†] Nagoya University.

[‡] CREST JST.

[§] Shimadzu Corporation.

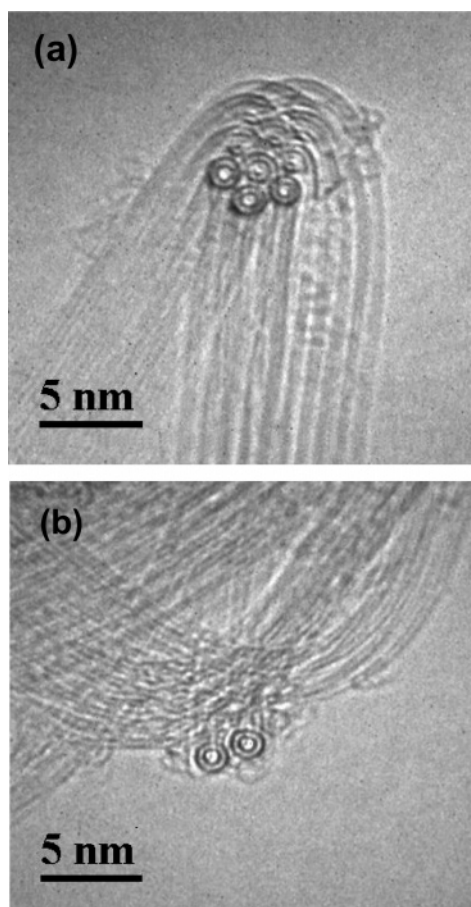


Figure 1. Typical TEM images of pure (90%) DWNTs oxidized at 700 °C.

250) for 1 h at 5–10 °C. The dispersed solutions were centrifuged (Hitachi Koki, Himac CS100 GXL) at 100 000g average for 1 h, and the supernatants were used in the PL measurements. The PL measurements were performed on a Shimadzu NIR-PL system (CNT-RF) equipped with a liquid N₂ cooled InGaAs detector array. The slit widths used were typically 20 nm for both excitation and emission. Absorption spectra were measured by using a JASCO V-570 spectrophotometer. Transmission electron microscopy (TEM) observation was carried out on a JEOL JEM-2100F. Solution Raman spectra were measured by using a Horiba Jobin Yvon HR-800 spectrometer. The 633-nm (1.96 eV) line from a He–Ne laser was used for excitation.

Results and Discussion

Photoluminescence from Inner Tubes of DWNTs. High-resolution TEM observation of the as-grown CCVD sample indicates that it is composed of SWNTs with a very small amount of DWNTs. The relative abundance of DWNTs with respect to SWNTs (i.e., DWNTs/(SWNTs + DWNTs)) was evaluated by counting the numbers of SWNTs and DWNTs from TEM images. The estimation indicated that the relative abundance of DWNTs (vs SWNTs) of the as-grown sample was ca. 1% (5/(396 + 5)). Furthermore, the relative abundance of DWNTs increases as the oxidation temperature increases. The relative abundances of DWNTs of the samples oxidized at 620, 670, and 700 °C were ca. 10% (22/(206 + 22)), ca. 70% (88/(33 + 88)), and ca. 90% (101/(7 + 101)), respectively. Namely, the relative yield of DWNTs can be varied between 1% and 90% by changing the oxidation temperature.

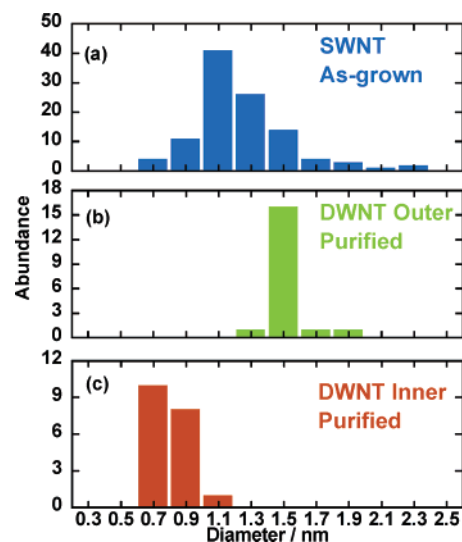


Figure 2. Diameter distributions from TEM observations. (a) SWNTs of the as-grown sample and (b) outer and (c) inner tubes of DWNTs of the sample oxidized at 700 °C. The average diameter of inner tubes of DWNTs is smaller than as-grown SWNTs and the residual SWNTs of the oxidized sample.

TABLE 1: The Wavelengths and Widths for Major Emission Peaks of Pure (90%) DWNT and As-Grown SWNTs^a

(n,m)	peak wavelength/nm			width/nm		
	as-grown (SWNT)	after the oxidation (DWNT)	Δ (SWNT – DWNT)	as-grown (SWNT)	after the oxidation (DWNT)	Δ (SWNT – DWNT)
(7,5)	1036	1033	3	23	20	3
(7,6)	1138	1135	3	34	36	–2
(9,4)	1118	1117	1	22	21	1
(8,6)	1188	1186	2	30	23	7

^a The slit widths used were 10 nm for both excitation and emission.

In the present samples, the average diameter of DWNTs of oxidized samples is very small as compared with that of CCVD-grown DWNTs reported^{3,6–8} as shown in Figure 1a and b. Figure 2 shows the diameter distributions of as-grown and oxidized samples at 700 °C estimated from TEM images. It is noticed that the average diameter of inner tubes of DWNTs (cf. Figure 2c) is smaller (0.8 nm) than that of the as-grown SWNTs (1.1 nm) (cf. Figure 2a). The average diameter of residual SWNTs in the oxidized sample (1.3 nm) is thicker than that of the as-grown SWNTs, because thin SWNTs are more reactive than thicker tubes toward oxidation in air. Since the diameter of C₆₀, the smallest fullerene, is 0.7 nm, the present DWNT is, in principle, the smallest DWNT so far synthesized by chemical vapor deposition.

Figure 3 shows a typical PL mapping of a purified DWNT (ca. 90%) sample obtained by oxidation at 700 °C. Contrary to our previous expectation, the major PL peak positions of the pure DWNT sample are almost identical to those of HiPco-SWNT/SDS/D₂O already reported.³⁰ As is seen in Figure 3, the PL due to the inner tubes with chiralities of (7,5), (7,6), and (9,4) is particularly enhanced. The major chirality of the inner tubes grown within the DWNTs is somehow very similar to that of the SWNTs, so that the tubes having the certain chirality are enhanced in the PL contour map irrespective of DWNTs and SWNTs. It is speculated that SWNTs and DWNTs have similar chirality dependence of intrinsic PL intensities.

Table 1 shows the main peak positions and the widths (in nm) observed from the present DWNTs and SWNTs samples.

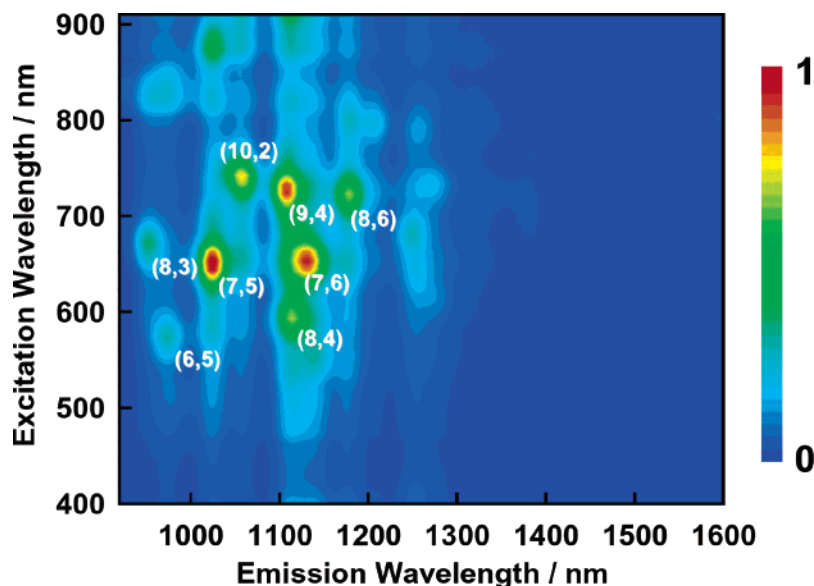


Figure 3. A contour plot of PL for the purified (90%) DWNT sample oxidized at 700 °C. The PL peaks of the DWNTs having inner tubes with chiralities of (7,5), (7,6), and (9,4) are particularly enhanced.

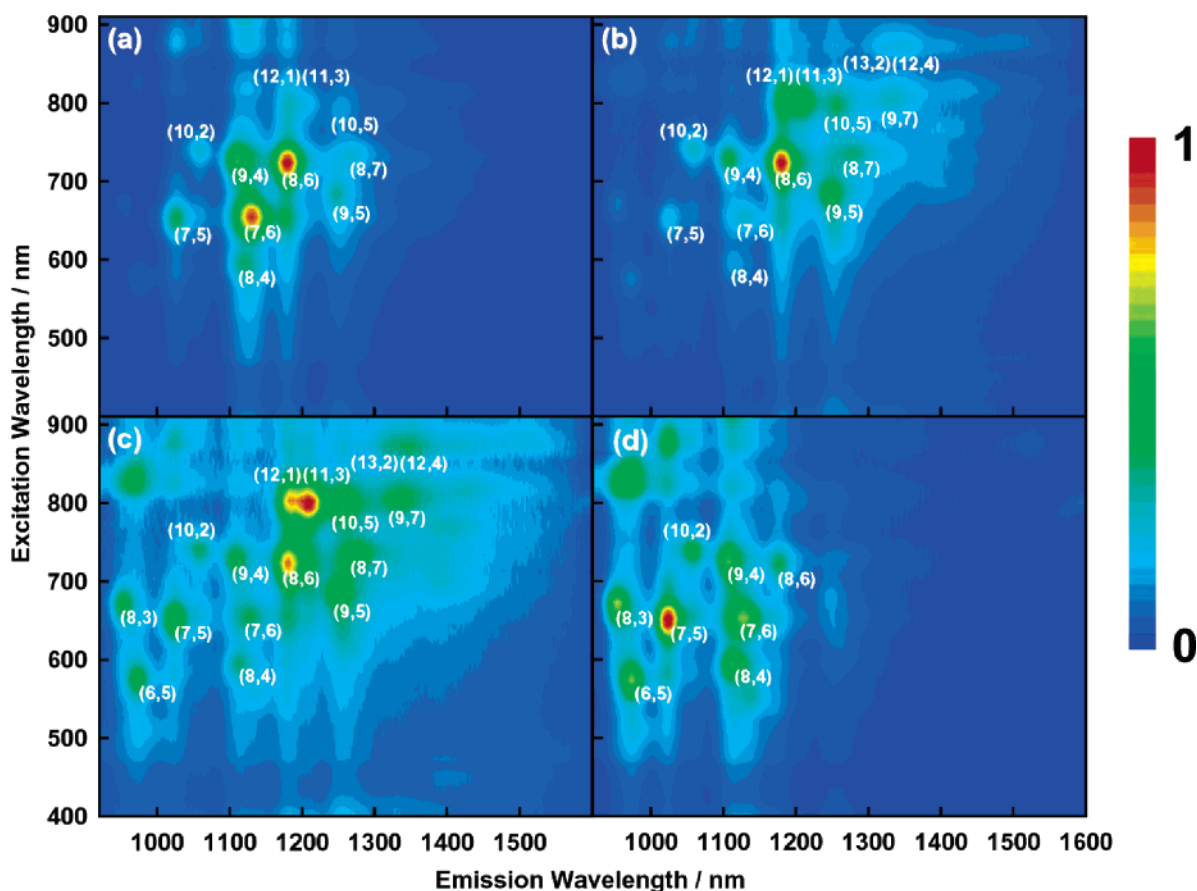


Figure 4. PL mappings of CCVD samples during the oxidation process of DWNTs (a) as-grown and oxidized at (b) 570 °C, (c) 620 °C, and (d) 670 °C. The PL peak distribution of SWNTs shifted to a thicker diameter region with increasing oxidation temperature. After oxidation at above 620 °C, new peaks corresponding to inner tubes of DWNTs appeared in a thinner diameter region such as (7,5), (7,6), (8,3), and (8,4).

The peak wavelengths of the tubes having chirality of (7,5), (7,6), (9,4), and (8,6) are obtained by curve fittings with a Lorentzian function. The PL peaks of DWNTs (90%) show 1–3 nm blue-shift with respect to the SWNT sample. It is well-known that emission and absorption wavelengths of SWNTs are oftentimes shifted in different dispersion environments.^{11,18–20} However, the observed shifts are smaller than those because of different environments. We think that the local fields for inner

tubes of the DWNTs are similar to those of the SWNTs and that the existence of outer tubes causes only minor effects to the local field for inner tubes than that of various surfactants. Another possibility is that the shifts originate from applying purification by thermal oxidation in air. It is not clear that the blue-shift originates from the differences between SWNTs and DWNTs or the purification. Table 1 shows that the widths of PL emission of the present DWNTs sample are 1–7 nm smaller

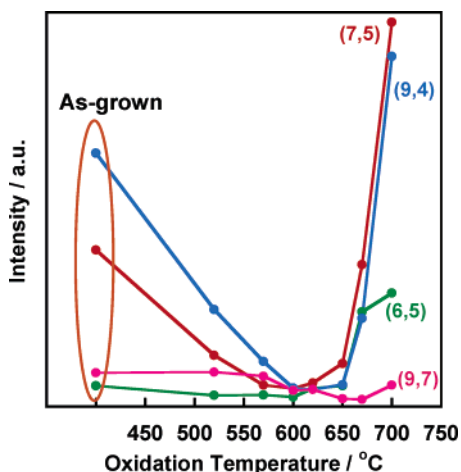


Figure 5. Oxidation temperature dependence of absolute PL intensities of (6,5), (7,5), (9,4), and (9,7).

than those of the as-grown SWNTs except for chirality of (7,6).

Chirality Determination of the Inner Tubes of DWNTs.

To confirm that the PL peaks from the pure (90%) DWNTs in Figure 3 are solely due to the inner tubes of the DWNTs (and not contaminated by the residual 10% SWNTs), we have conducted a detailed temperature-dependent thermal oxidation experiment on the samples of various mixing ratios of DWNT and SWNT and have seen the PL spectral changes during the oxidation.

Figure 4 shows PL measurements of the CCVD nanotube samples during the oxidation process of DWNTs. The PL contour mapping of as-grown sample shows several peaks because of SWNTs with chiralities such as (7,6) and (8,6) (cf. Figure 4a), since the majority of the as-grown CNTs here is SWNTs. PL peak distribution starts to shift, however, to a thicker diameter (i.e., upper-right) region in the map as oxidation temperature increases, because SWNTs with smaller diameters are more reactive against oxidation than thicker tubes (cf. Figure 4b). In the sample oxidized at 620 °C (cf. Figure 4c), new peaks due to nanotubes with chiralities of (7,5), (8,3), and (6,5) appear in a thinner diameter (i.e., lower-left) region. These peaks can be identified as signals from inner tubes of DWNTs, since as the diameter distributions in Figure 2 show, the mean diameter of the inner tubes of the present DWNTs is much smaller than those of as-grown SWNTs and residual SWNTs in the oxidized sample.

By further removing SWNTs from the sample by oxidation, distinct signals PL from inner tubes of DWNTs are observed separately from those of SWNTs as shown in Figure 4c and d. These signals are due to DWNTs with chiralities such as (6,5), (7,5), (7,6), (8,3), and (8,4). The thermal oxidation at a higher temperature of 700 °C provides pure (90%) DWNTs, so that the corresponding PL peaks are almost only from inner tubes of DWNTs (cf. Figure 3). At the same time, signals from residual SWNTs disappear almost completely in the PL mapping as shown in Figure 3. In addition, PL distribution of DWNTs also shifts to a thicker diameter region in the contour map (cf. Figures 3 and 4d).

Figure 5 shows absolute intensities of several PL peaks as a function of oxidative treatment temperature. Chiralities of (7,5) and (9,4) show strong emission in the as-grown sample compared with those of (6,5) and (9,7). PL intensities of chiralities of (6,5), (7,5), and (9,4) decrease with increasing oxidation temperature less than 570 °C corresponding to burning of thinner SWNTs. On the other hand, the PL intensity of a

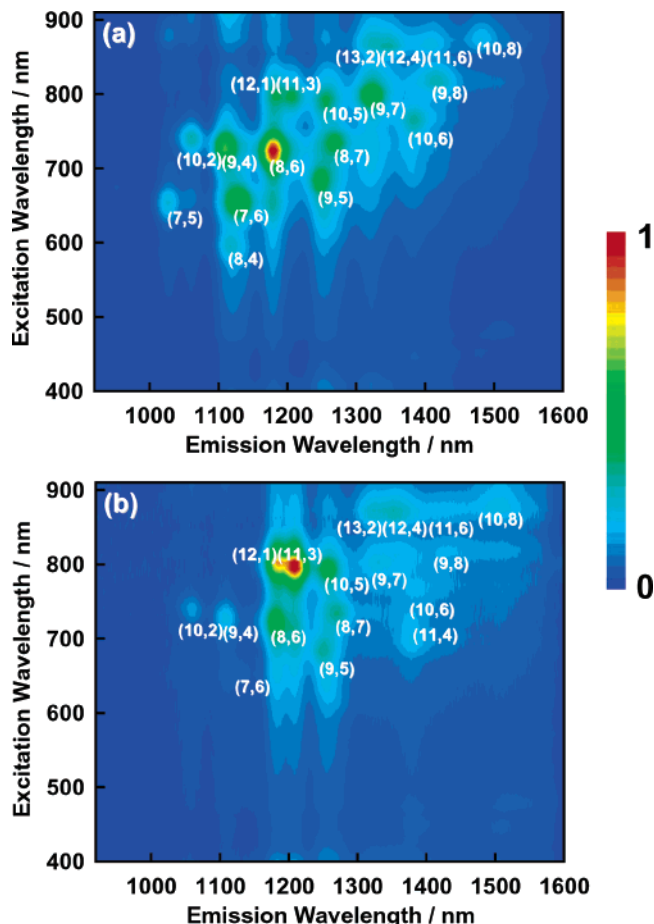


Figure 6. PL mappings of HiPco-SWNTs (a) before and (b) after oxidation. PL distribution only shifts to a thicker diameter region after the oxidation.

chirality of (9,7) increases with increasing oxidative treatment temperature less than 570 °C. Further oxidation increases PL intensities of chiralities of (6,5), (7,5), and (9,4) corresponding to inner tubes of DWNTs while decreases that of a chirality of (9,7).

To further ensure that the observed PL signals for the purified (90%) DWNT sample (cf. Figure 3) stem exclusively from inner tubes of DWNTs, similar temperature-dependent oxidation experiments were carried out on HiPco-SWNTs where no DWNTs are present in the sample. HiPco-SWNTs were oxidized at 640 °C for a short period of 5 min, because an extended oxidation as employed in the above zeolite-CCVD samples leads to the complete combustion of HiPco-SWNTs. Figure 6 shows PL contour maps of HiPco-SWNTs before (a) and after (b) the thermal oxidation. The PL distributions shift to thicker diameter region after the oxidation since SWNTs with smaller diameters are weaker than thicker tubes against oxidation. Unlike the zeolite-CCVD samples, no new peaks in smaller diameter regions appear after the oxidation in the HiPco-SWNTs sample, and here the thermal oxidation only removes SWNTs with smaller diameters in the intact sample. This again confirms that the new peaks which appeared in the smaller diameter region after the oxidation at 700 °C in Figure 3 originate from the inner tubes of DWNTs.

Thermal Durability of DWNTs against SWNTs. By comparing the oxidation experiments on zeolite-CCVD samples with that of HiPco, the observed changes of PL mappings during the oxidation process correspond to the changes of diameter distribution during the oxidation. Interestingly, SWNTs having

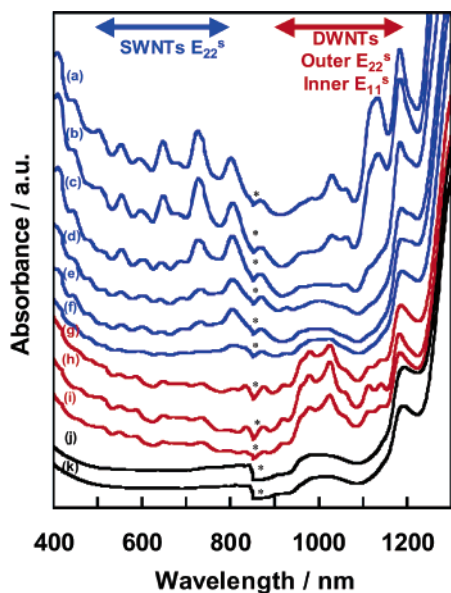


Figure 7. Oxidation temperature dependence of absorption spectra of DWNTs/SWNTs samples (a) as-grown and oxidized at (b) 520 °C, (c) 570 °C, (d) 600 °C, (e) 620 °C, (f) 650 °C, (g) 670 °C, (h) 700 °C, and (i) 720 °C. The spectra of SWNT rich samples (Figure 7a–f) and DWNT enriched samples (Figure 7g–i) are colored in blue and red, respectively. Blue arrow shows E_{22}^s region of SWNTs in the SWNT rich samples (Figure 7a–f). Red arrow indicates E_{11}^s of inner and E_{22}^s of outer tubes of enriched DWNTs, which overlap each other in 900–1200 nm region (Figure 7g–i). These spectra are not corrected with that of sodium cholate/D₂O baseline. Absorption spectra of (j) sodium cholate/D₂O solution and (k) that with H₂O (100 μ L of H₂O in 6 mL of the solution) are also shown (black lines). The asterisks indicate the step due to the change of the detector.

(12,1) and (11,3) chiralities exhibit enhanced peaks in the contour map even after the oxidation in both the zeolite-CCVD and HiPco cases as shown in Figures 4c and 6b. This suggests that SWNTs having (12,1) and (11,3) chiralities are somehow much more robust toward oxidation than other SWNTs.

Figure 7a–i shows absorption spectra of zeolite-CCVD samples during the oxidation process. Absorption spectra of 100 mM sodium cholate/D₂O solution are also shown in Figure 7j for comparison. The peaks around 500–800 nm shift systematically to longer wavelengths with increasing oxidation temperature because the diameter distributions of SWNTs shift to thicker diameter region.^{28,29} At the oxidation above 670 °C, new signals appear around 900–1200 nm as shown in Figure 7g–i. Assuming that the diameters of inner and outer of DWNTs are 0.7–1.0 nm and 1.4–1.8 nm, respectively, these peaks can be assigned to E_{22}^s of outer tubes and to E_{11}^s of inner tubes of DWNTs, which are known to overlap each other in this region.^{13,30}

Sodium cholate/D₂O solution used also shows a weak and broad absorption feature in the 950–1100 nm region as in Figure 7j, and this absorption feature might be changed by the existence of impurity H₂O in the solution. However, careful blank experiments with small amounts of H₂O added to the sodium cholate/D₂O solutions do not alter the absorption feature around 950–1100 nm (cf. Figure 7j and k), indicating that the observed signals around 950–1100 nm in Figure 6g, h, and i stem solely from DWNTs.

Figure 8 shows solution Raman spectra of the present samples during the temperature-dependent oxidation process of DWNTs in the radial breathing mode (RBM) region. In the SWNT rich samples, the peak distributions shift systematically to a lower wavenumber region as oxidation temperature increases, indicat-

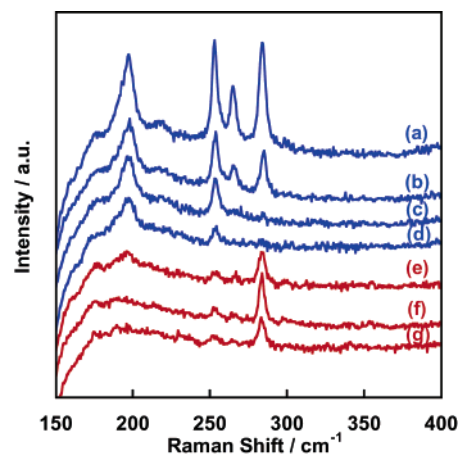


Figure 8. Solution Raman spectra of CCVD samples during the temperature-dependent oxidation process of DWNTs in the radial breathing mode (RBM) region (a) as-grown and oxidized at (b) 520 °C, (c) 570 °C, (d) 620 °C, (e) 670 °C, (f) 700 °C, and (g) 720 °C. The spectra of SWNT rich samples (Figure 8a–d) and DWNT enriched samples (Figure 8e–g) are colored in blue and red, respectively. Excitation wavelength is 632.8 nm.

ing that the diameter distributions of SWNTs shift to a thicker diameter (cf. Figure 8a–d). As shown in Figure 8e–g, Raman spectra of the DWNT enriched samples oxidized at a temperature above 670 °C show a salient peak at 284 cm^{-1} corresponding to an inner tube of DWNTs, and the peaks observed between 200 and 260 cm^{-1} because of SWNTs decrease dramatically.

Conclusions

In this article, photoluminescence from inner tubes of pure (90%) DWNTs has been reported. This is confirmed by careful temperature-dependent thermal oxidation experiments on samples with various mixing ratios of DWNTs and SWNTs, where PL distributions due to DWNTs and SWNTs shift sensitively but independently with each other in the contour map. The PL from inner tubes of DWNTs with chiralities of (7,5), (7,6), and (9,4) are particularly enhanced.

Acknowledgment. We thank Professor R. Saito (Tohoku University), Dr. S. Irlé (Emory University), and Dr. Y. Ohno (Nagoya University) for their helpful discussions. This work has been supported by the JST CREST Program for Novel Carbon Nanotube Materials and the 21st century COE program of JSPS.

References and Notes

- (1) Sugai, T.; Yoshida, H.; Shimada, T.; Okazaki, T.; Shinohara, H.; Bandow, S. *Nano Lett.* **2003**, *3*, 769.
- (2) Flahaut, E.; Bacsá, R.; Peigney, A.; Laurent, C. *Chem. Commun.* **2003**, 1442.
- (3) Hiraoka, T.; Kawakubo, T.; Kimura, J.; Taniguchi, R.; Okamoto, A.; Okazaki, T.; Sugai, T.; Ozeki, Y.; Yoshikawa, M.; Shinohara, H. *Chem. Phys. Lett.* **2003**, *382*, 679.
- (4) Ago, H.; Nakamura, K.; Imamura, S.; Tsuji, M. *Chem. Phys. Lett.* **2004**, *391*, 308.
- (5) Endo, M.; Muramatsu, H.; Hayashi, T.; Kim, Y. A.; Terrones, M.; Dresselhaus, M. S. *Nature* **2005**, *433*, 476.
- (6) Ramesh, P.; Okazaki, T.; Taniguchi, R.; Kimura, J.; Sugai, T.; Sato, K.; Ozeki, Y.; Shinohara, H. *J. Phys. Chem. B* **2005**, *109*, 1141.
- (7) Ramesh, P.; Okazaki, T.; Sugai, T.; Kimura, J.; Kishi, N.; Sato, K.; Ozeki, Y.; Shinohara, H. *Chem. Phys. Lett.* **2006**, *418*, 408.
- (8) Ramesh, P.; Sato, K.; Ozeki, Y.; Kishi, N.; Sugai, T.; Shinohara, H. *Nano* **2006**, *1*, 47.
- (9) Kurachi, H.; Uemura, S.; Yotani, J.; Nagasako, T.; Yamada, H.; Ezaki, T.; Maesoba, T.; Loutfy, R.; Moravsky, A.; Nakazawa, T.; Katagiri, S.; Saito, Y. *Asia Display/IDW'01* **2001**, 1237.

- (10) Shimada, T.; Sugai, T.; Ohno, Y.; Iwatsuki, S.; Kishimoto, S.; Mizutani, T.; Bandow, S.; Yoshida, H.; Okazaki, T.; Shinohara, H. *Appl. Phys. Lett.* **2004**, *84*, 2412.
- (11) Hertel, T.; Hagen, A.; Talalaev, V.; Arnold, K.; Hennrich, F.; Kappes, M.; Rosenthal, S.; McBride, J.; Ulbricht, H.; Flahaut, E. *Nano Lett.* **2005**, *5*, 511.
- (12) Shimada, T.; Miyauchi, Y.; Sugai, T.; Shinohara, H.; Maruyama, S. *NT05* **2005**, VI-3.
- (13) Kalbáč, M.; Kavan, L.; Zukalová, M.; Dunsch, L. *Adv. Funct. Mater.* **2005**, *15*, 418.
- (14) O'Connell, M. J.; Bachilo, S. M.; Huffman, C. B.; Moore, V. C.; Strano, M. S.; Haroz, E. H.; Rialon, K. L.; Boul, P. J.; Noon, W. H.; Kittrell, C.; Ma, J.; Hauge, R. H.; Weisman, R. B.; Smalley, R. E. *Science* **2002**, *297*, 593.
- (15) Bachilo, S. M.; Strano, M. S.; Kittrell, C.; Hauge, R. H.; Smalley, R. E.; Weisman, R. B. *Science* **2002**, *298*, 2361.
- (16) Miyauchi, Y.; Chiashi, S.; Murakami, Y.; Hayashida, Y.; Maruyama, S. *Chem. Phys. Lett.* **2004**, *387*, 198.
- (17) Heller, D. A.; Mayrhofer, R. M.; Baik, S.; Grinkova, Y. V.; Usrey, M. L.; Strano, M. S. *J. Am. Chem. Soc.* **2004**, *126*, 14567.
- (18) Moore, V. C.; Strano, M. S.; Haroz, E. H.; Hauge, R. H.; Smalley, R. E. *Nano Lett.* **2003**, *3*, 1379.
- (19) Lefebvre, J.; Fraser, J. M.; Homma, Y.; Finnie, P. *Appl. Phys. A* **2004**, *78*, 1107.
- (20) Okazaki, T.; Saito, T.; Matsuura, K.; Ohshima, S.; Yumura, M.; Iijima, S. *Nano Lett.* **2005**, *5*, 2619.
- (21) Wang, F.; Dukovic, G.; Brus, L. E.; Heinz, T. F. *Science* **2005**, *308*, 838.
- (22) Mukhopadhyay, K.; Koshio, A.; Tanaka, N.; Shinohara, H. *Jpn. J. Appl. Phys.* **1998**, *37*, L1257.
- (23) Mukhopadhyay, K.; Koshio, A.; Sugai, T.; Tanaka, N.; Shinohara, H.; Konya, Z.; Nagy, J. B. *Chem. Phys. Lett.* **1999**, *303*, 117.
- (24) Okamoto, A.; Kawakubo, T.; Hiraoka, T.; Okazaki, T.; Sugai, T.; Shinohara, H. Structural and Electronic Properties of Molecular Nanostructures. *AIP Conf. Proc.* **2002**, *633*, 194.
- (25) Okamoto, A.; Kawakubo, T.; Hiraoka, T.; Okazaki, T.; Sugai, T.; Shinohara, H. *Mol. Cryst. Liq. Cryst.* **2002**, *387*, 317.
- (26) Okamoto, A.; Shinohara, H. *Carbon* **2005**, *43*, 431.
- (27) Maruyama, S.; Kojima, R.; Miyauchi, Y.; Chiashi, S.; Kohno, M. *Chem. Phys. Lett.* **2002**, *360*, 229.
- (28) Nagasawa, S.; Yudasaka, M.; Hirahara, K.; Ichihashi, T.; Iijima, S. *Chem. Phys. Lett.* **2000**, *328*, 374.
- (29) Zhou, W.; Ooi, Y. H.; Russo, R.; Papanek, P.; Luzzi, D. E.; Fischer, J. E.; Bronikowski, M. J.; Willis, P. A.; Smalley, R. E. *Chem. Phys. Lett.* **2001**, *350*, 6.
- (30) Weisman, R. B.; Bachilo, S. M. *Nano Lett.* **2003**, *3*, 1235.